ACCEPTED MANUSCRIPT

Final published version of this article:

Self-limiting Sb monolayer as a diffusion source for Ge doping

Sgarbossa F., Maggioni G., Rizzi G.A., Carturan S.M., Napolitani E., Raniero W., Carraro C., Bondino F., Píš I., De Salvador D

Applied Surface Science, Volume 496, 1 December 2019, 143713

Available online 20 August 2019, Version of Record 26 August 2019.

DOI: https://doi.org/10.1016/j.apsusc.2019.143713

© 2019. This manuscript version is made available under the CC-BY-NC-ND 4.0 license http://creativecommons.org/licenses/by-nc-nd/4.0/

*Revised manuscript (unmarked)
Click here to view linked References

Self-limiting Sb monolayer as a diffusion source for Ge doping

Francesco Sgarbossa[1,2]; Gianluigi Maggioni[1,2]; Gian Andrea Rizzi[3]; Sara Maria Carturan[1,2]; Enrico Napolitani[1,2]; Walter Raniero[2]; Chiara Carraro[1,2]; Federica Bondino[4]; Igor Píš[4,5]; Davide De Salvador*[1,2];

1) Department of Physics and Astronomy, Università degli Studi di Padova, Via Marzolo n. 8, 35131 Padova, Italy

2) Istituto Nazionale di Fisica Nucleare, Laboratori Nazionali di Legnaro, Viale dell'Università n. 2, 35020 Legnaro (PD), Italy

3) Department of Chemical Sciences and INSTM unit, Università degli Studi di Padova, Via Marzolo n. 1, 35131 Padova, Italy

4) IOM-CNR Laboratorio TASC, S.S. 14 km 163.5, 34149 Basovizza, Trieste, Italy

5) Elettra – Sincrotrone Trieste S.C.p.A., S.S. 14 km 163.5, 34149 Basovizza, Trieste, Italy

*e-mail: davide.desalvador@unipd.it

Abstract

A new method for the creation of high-quality, fully electrically active junctions to be applied in nanostructured semiconductor materials is explored in this work. The method consists in a gas phase antimony deposition on Ge, which gives rise to an antimony self-limiting behavior to form a monolayer (ML) on the Ge (100) surface. The ML formation is characterized by a wide thermal process window in terms of time and temperature. Synchrotron radiation Angle Resolved X-Ray Photoelectron Spectroscopy shows that the ML structure consists in oxidized Sb grown over a very thin layer of Ge oxide, and a small amount of metallic Sb is embedded beneath the Ge surface during the deposition process. Interestingly, during the ML formation process native Ge oxide is reduced without the need of strong acid pre-treatments. By performing further thermal annealing in equilibrium conditions, Sb diffusion can be faithfully described by a well assessed diffusion model. Finally, processing the Sb monolayer with Pulsed Laser Melting technique, which is a strongly out-equilibrium diffusion process, allows to exploit the entire Sb ML as a dopant source, thus achieving junctions with a very high dopant concentration (1.2×10^{20} cm^{-3} Sb surface concentration) and a 100% Sb electrical activation.

Keywords: Monolayer, Antimony, Germanium, Doping, Surface Chemistry

Introduction

One of the main goals in the semiconductor research is the production of a shallow junction conformal to the surface of a device. This request emerges from the increasing importance of nanostructured devices made by semiconductor materials like multi-gate transistors. The 3D

geometry of these devices implies the capability to dope the semiconductor material in a nanostructured, non-planar geometry, which continues to be a difficult task, as reported in the latest ITRS roadmap [1].

The main task required for this scope is the ability to have a conformal source of dopant combined with an appropriate doping technique that promotes the injection of the dopant into the structure. Furthermore, the control of the amount of the dopant source “in situ” is another crucial aspect since it directly affects the process reproducibility and it allows to finely control the diffused amount of dopant.

One of the most promising techniques for the deposition of a well-defined amount of dopant is the use of self-limiting chemical deposition that is the basis of the monolayer doping technique (MLD). This particular approach consists in depositing a monolayer of a molecular precursor by a self-limited surface adsorption reaction, which leads to a chemi- or physisorbed mono- or multi- layer. This layer acts as a dopant source after a thermal degradation of the adsorbed molecules by the release of the doping atomic species that diffuses inside the substrate. This new technique allows to dope not only 3D nanostructured materials [2] with an intrinsically conformal method, but also flat semiconductor surfaces by avoiding the ion implantation technique and the consequent damage of the crystal lattice [3].

Thanks to a wide set of surface chemical reactions involving different semiconductors and different precursors, the MLD technique is in principle very versatile as shown by its successful application to commonly used semiconductors, such as silicon [4]. Nevertheless, the wide range of available molecular precursors is strongly narrowed by specific requirements such as a good self-limiting behaviour, a thermal decomposition and a thermal release of the doping atomic species within a proper temperature range, normally limited by either the dopant diffusivity or the semiconductor melting point [5]. Moreover, the chemical structure of the molecular precursor plays a crucial role: if the use of a specific functional group is directly related with the reactivity towards a semiconductor surface, the rest of the molecule moiety should be selected both to guarantee a thermal decomposition of the molecule and to avoid the diffusion of contaminant species inside the semiconductor, that can give rise to a dopant deactivation or clustering.

Nowadays the monolayer doping is a well-studied technique with silicon substrates [4] and the formation of ultra-shallow junctions is proved in literature [6]; moreover, also an ultra-shallow junction monolayer doping FinFET transistor has been implemented on silicon substrates [7].

More recently, a modification of the monolayer doping technique was presented in literature [8,9]: the new idea is to form a dopant-containing ML on a source substrate (also called donor substrate), different from the target substrate. The two substrates are put in contact and by means of a thermal annealing, the dopant diffuses in both substrates. This method is called monolayer contact doping and presents several advantages such as the avoiding of the formation and the removal of a capping layer, or the possibility to use different surface reactions by using a different donor substrate material respect to the target.

Moreover, a non-contact doping technique variation has been proposed in last years, called remote monolayer doping, based on thermal fragmentation of dopant-containing monolayers and evaporation processes, promoting a controlled doping process fully compatible with large scale direct patterning, as proposed by Hazut and co-workers [10].

The use of these techniques on germanium is still quite unexplored [5,11,12], but the arising of germanium based devices and nanostructures[13,14] makes these studies more and more appealing. In the last years, germanium has been re-considered as semiconducting material [15] due to its small band gap, high mobility of charge carriers and the possibility to obtain a direct band gap material by the controlled use of strain (also the strain induced by a heavily doped region) [16,17].

These germanium properties promoted the research in a wide range of application fields from photovoltaics[2] to nanoelectronics[14], radiation detectors[18] and opto-plasmonics[19,20].

In this paper we investigate a new monolayer (ML) deposition technique aimed at the adsorption and diffusion of antimony in germanium. The Sb affinity to Ge surfaces is already known in literature[21,22], but the formation of Sb ML on Ge has been studied only on Ge (111) surfaces, in an ultra-high vacuum deposition condition and without the demonstration of a self-limiting deposition behaviour[22]. The new technique proposed here exploits a self-limited, gas phase atomic deposition, obtained following a thermally-induced sublimation of Sb atoms from a solid source placed near the Ge surface. This approach allows us to completely avoid wet chemical reactions and the consequent issues related to the synthesis and the use of Sb based molecular precursors. We demonstrate that antimony chemisorbs on Ge (100) and the deposition involves a self-limited process, which leads to the formation of a single Sb monolayer (referred to the atomic surface density of Ge (100), i.e. 6.25×10^{14} cm^{-2}). The Ge (100) face was chosen as the most used in semiconductor industries and applications. We examine the self-limiting behaviour in a wide range of deposition times and temperatures by monitoring the deposited Sb doses by Rutherford Backscattering Spectrometry in channelling conditions (c-RBS). The Sb depositions are also chemically characterized with X-Ray Photoelectron Spectroscopy (XPS). The photoemission spectra are acquired at different take-off angles and the angle variation of the peak intensity is modelled with an Angle Resolved XPS analysis to obtain information on the depth distribution of different XPS signals.
The Sb ML is tested as a source of dopant and for this reason different diffusion treatments are used. Some samples are annealed with rapid thermal processes and others are treated with a non-equilibrium technique called Pulsed Laser Melting (PLM), as described in the experimental section.
Finally, treated samples are characterized with Secondary Ion Mass Spectrometry (SIMS) to verify the antimony diffusion inside the semiconductor and the electrical Sb activation is monitored by four-point probe Van der Pauw-Hall measurements.

Experimental

Sample preparation

A double polished p-doped Ge (100) wafer (supplied by Umicore) was cut in 1x1 cm^2 and 1x2 cm^2 samples and cleaned with hot 2-propanol in order to remove dicing residuals.
In order to have an antimony source, Sb was deposited on a Si (100) substrate via RF sputtering deposition: the silicon substrates were put in a stainless-steel vacuum chamber, evacuated to a base pressure lower than 1×10^{-4} Pa. Either 20 or 100 nm of metallic Sb (99.9999% purity supplied by ACI Alloys) were deposited on Si substrates by a RF magnetron sputtering equipment (30 W, 13.56 MHz). The sputtering deposition rates were derived by monitoring the deposited thickness via RBS analysis[23]. The Sb source on Si were 8x25 mm^2 for the 100 nm sources used in tubular furnace, and 5x10 mm^2 for 20 nm sources used in RTA furnace.

Gas phase depositions

The antimony depositions on Ge substrates were made in two different furnaces: a standard tubular furnace equipped with a quartz tube for vacuum and gas flux treatments, and a Jipelec JetFirst Rapid Thermal Processing machine (RTA). The former had a maximum heating ramp of 3 °C s^{-1} in fast annealing use (i.e. by rapid insertion and removal of the sample in the pre-heated furnace [24]) and the latter heating ramp was 100-150°C s^{-1}. The sample temperature was monitored by a thermocouple connected with the sample boat in the standard furnace and by a calibrated

pyrometer, which measured the temperature of a supporting Si wafer in the RTA system. Before any deposition, both the furnace and RTA were cleaned with five cycles of vacuum and N_2 refill.
In the standard furnace, the Sb-coated Si substrate was placed on two spacers over a Ge target, with the Sb-deposited face in front of Ge target at a distance of 8 mm, as schematized in Figure 1. The whole system was placed in a quartz boat to be entered into the furnace. More details are reported in a recent work [23].

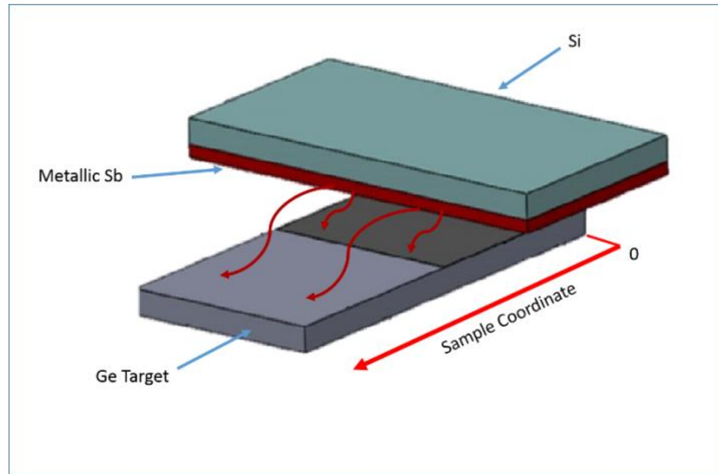

Figure 1 *Configuration used for the Sb deposition in a standard furnace.*

The tubular furnace was used only for 30 minutes treatments, while RTA was used for shorter annealing, from 30 minutes down to 10 s.
In RTA, the Si source and Ge sample were placed side by side on the supporting wafer with upward sputtered Sb source and Ge depositing surface both looking at the heating lamps. Quartz spacers were added in order to confine the deposition area from the all furnace chamber (see additional information Figure 1). This geometry is functional to the cold wall furnace that guarantees heating homogeneity of samples placed on the supporting wafer in front of the lamps. The effect of the difference of Ge emissivity with respect to silicon, and the impact of quartz spacers were computed in a finite element thermal simulation of the system. Temperature differences lower than 10°C with respect to the unperturbed system and no significant effects on the ramp were estimated. Annealing times as short as 10 s can be achieved with this set-up.

Antimony ML diffusion

Rapid Thermal Annealing (RTA) and Pulsed Laser Melting (PLM) techniques were also used without Sb on Si source to test the diffusion processes in a second step treatment of the Sb pre-deposited on Ge.
A Nd:YAG laser (Quantel YG981) with a single pulse of 7 ns and a threefold frequency (wavelength equal to 355 nm) is used in PLM technique. The germanium surface is melted in the 7 mm circular spot of the laser, owing to the high energy density, around 400 mJ cm^{-2}. After a certain thermal dissipation delay (around 30 ns) the Ge epitaxially regrows and the Sb ML diffused in liquid Ge is englobed in the crystal lattice. Thanks to the extremely fast regrowth, the technique has proven to be very effective in doping Ge at concentrations even above the solubility limits[25–27].

Characterization techniques

The antimony monolayer on Ge and the metallic antimony source deposited on Si were

characterized by Rutherford Backscattering Spectrometry in channelling condition (c-RBS). These measurements were carried out using 2.0 MeV $^{4}He^{+}$ beam at the Van de Graaff accelerator at the INFN *Laboratori Nazionali di Legnaro* with a 160° scattering angle. Ge substrate was aligned in axial channelling condition to minimize the bulk signal causing pileup background. In this way the superficial Sb doses were determined with a high sensitivity (see Figure 2 of additional info).

Sb diffusion inside Ge was characterized with Secondary Ion Mass Spectrometry (SIMS) Cameca ims-4f with a $^{133}Cs^{+}$ primary ion beam rastered over a 250x250 μm^2 area while $^{133}Cs^{121}Sb^{+}$ secondary ions are collecting from a central circular area of 150 μm^2. The antimony calibration was performed by measuring a Ge standard with a known implanted Sb dose, with an accuracy of 10% in dose. The depth calibration was performed by measuring the SIMS crater depth with a profilometer and assuming a constant sputtered rate. The accuracy of this measure is about 2%. SIMS measurements are complementary to RBS ones: the presence of Sb deeper than 10 nm is detectable by the former while Sb areal density in the first 10 nm by the latter.

X-Ray Photoelectron Spectroscopy (XPS) measurements were conducted at the Elettra Synchrotron facility in Basovizza (Trieste, Italy) at the BACH beamline with a VG Scienta R3000 electron analyzer placed at 60° from the beam direction. All the XPS spectra were calibrated using the Au 4f 7/2 core level peak from a reference. The angle-resolved XPS (AR-XPS) data were analysed and modelled with a multi-layer code named BRIXIAS package developed by Drera at al.[28 29].

AFM images were performed on Ge surfaces by a *DI Cp-II* AFM instrument using a commercial silicon nitride cantilever.

The electrical characterizations were carried out with a four-probe electrical apparatus according to the Van der Pauw-Hall method. The system (supplied by MMR Technologies) consists in a vacuum chamber containing four Au tips connected with a Keithley 2600 source-meter and a switch matrix in order to perform sheet resistance and carrier concentration Hall measurements, controlled by a home-made software. For the carrier concentration measurements, the system is equipped with a 0.65 T permanent magnet [30].

Results and Discussion

Study of deposition parameters: temperature and time dependence

The antimony deposition on Ge (100) was first studied in a wide temperature range, from 400°C to 790°C, by using a standard tubular furnace and setting 1800 s as deposition time. A 100-nm-thick metallic Sb source deposited on Si was used as described in the experimental section.
The functionalized Ge samples were analysed with Rutherford Backscattering Spectrometry in channelling condition (c-RBS), by mapping each sample with 0.5 x 0.5 mm^2 beam to measure the Sb 2D distribution on Ge surface. The Sb source on Si was measured as well, in order to evaluate the source state and the Sb consumption at the end of the deposition treatments.

Thanks to the c-RBS measurements, the Sb behaviour on Ge (100) surface at different temperature can be easily monitored, and the Sb areal density deposited on Ge is reported in Figure 2 as a function of deposition temperature (a) and time (b).

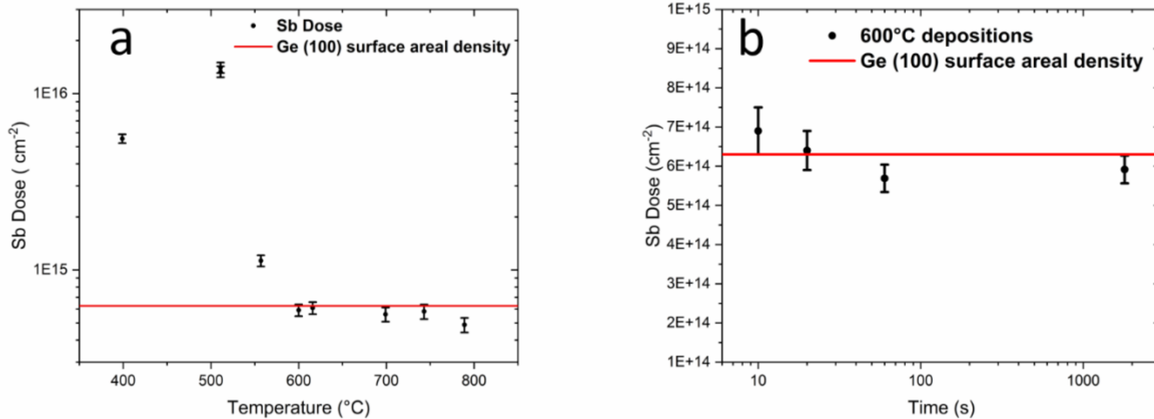

Figure 2a *c-RBS Sb doses on Ge (100) surface as a function of the deposition temperature. All these processes were 30 min-long, starting from a 100 nm Sb on Si source. The Sb dose shown in this figure is referred to a Sb dose at 2 mm from the sample edge.*

Figure 2b *c-RBS Sb doses on Ge (100) surface as a function of the duration of the process; these data are referred to RTA deposition at 600°C, starting from a 20 nm Sb on Si source.*

It can be observed in Figure 2a that Sb areal density increases going from 400°C to 510°C, then decreases and stays approximately constant between 600°C and 750°C with a slight decrease at the highest 790°C temperature. It is worth to note that the constant plateau is close to the value of the Ge monolayer atomic density indicated by a red line as a reference (6.25x 10^{14} at cm^{-2}).
By the analyses of the Sb source we notice that the 100-nm-thick Sb film is only partially consumed at 400°C while it is almost exhausted at 510°C and no trace is found at higher temperatures. The increase of Sb on Ge going from 400°C to 510° (Fig. 2a) is therefore due to the increased availability of Sb that evaporates faster at higher temperature. A different phenomenon is revealed at even higher temperature when the Sb source is exhausted: the 560°C deposition reveals a net decrease of the Sb, meaning that the Sb deposition is not stable at higher temperature after source exhaustion. This instability does not apply to the first monolayer of the deposit that remains stable between 600° up to 750°C, showing a clear self-limiting behaviour.
It is evident that Sb deposited on top of the first monolayer displays a different thermodynamic stability with respect to Sb directly bound to Ge surface. Furthermore, it is worth to note that at the same temperature Sb is not stable on the Si surface, as proved by the complete removal of Sb from the Si surface (reported in additional info Figure 2b), whereas the layer is stable on Ge surface (Figure 2a of additional info). This indicates that a specific interaction between Sb and Ge surface occurs, as it will be investigated in depth in the following sections.
The second important deposition parameter is the duration of the process. The temperature that we decided to use for this process is the lowest temperature that ensures a self-limiting behaviour and a good uniformity and for these reasons 600°C was chosen. In the RTA furnace, the duration of the process can be diminished down to a few s, allowing us to explore the minimal duration of the process.
A 20 nm-thick metallic Sb thick source has been used to scale down the treatment time to avoid the waste of Sb and to minimize the Sb dispersed inside the chamber.

Figure 2b shows the Sb doses detected with c-RBS on Ge target sample after a certain treatment time. It is evident that the ML formation is a very fast process, which is already accomplished within the first 10 s.
The Sb distribution on the Ge surface was also investigated by measuring the Sb dose as a function of the position along the sample (sample coordinate). Figure 3 shows the results of these measurements for the depositions at temperatures ranging from 400°C to 790°C.

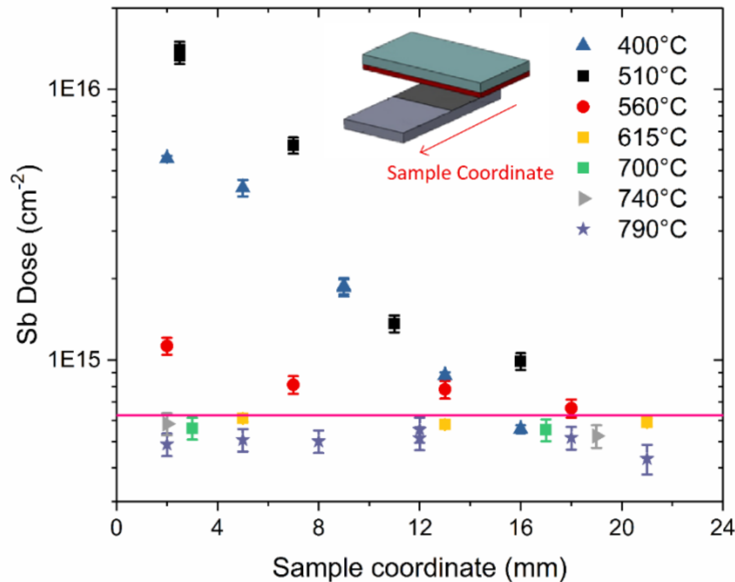

***Figure 3** Antimony RBS doses plotted as a function of the position along the Ge substrate (sample coordinate). The results coming from depositions at different deposition temperatures are reported with colored points, ranging from 400°C to 790°C; all the deposition treatments are 30 minutes long with the same tubular furnace. The red line is the Ge (100) surface atomic density (used as a reference level).*

The reported data point out that processes carried out at T < 600°C show a Sb dose gradient toward the source, while a very uniform deposition along the surface is obtained in the range 600-790°C. This high uniformity is also found in shorter RTA depositions (see, as an example, Figure 3 of additional info). This finding is a crucial point in the perspective of doping applications: the self-limiting regime that is obtained in the latter thermal window guarantees a high homogeneity of the Sb distribution in a final device.
To verify the layer uniformity at lower scale, surface AFM images (5x5 μm^2) on untreated Ge wafer and after 1 minute at 600°C monolayer deposition on Ge were performed (reported in additional info), revealing negligible surface roughness differences, eventually caused by the deposition process. This observation excludes any antimony oxide surface aggregation, that is not detectable by c-RBS technique and strengthens the existence of a specific surface interaction between germanium and antimony that generates the self-limiting behavior of the process.

In summary, a spatially uniform Sb ML has been detected, and time-temperature formation parameters have been studied showing a very rapid and uniform formation process.

AR-XPS Surface Analysis

After the RBS studies of Sb deposition process parameters, we characterized the Sb ML with XPS analysis to verify the surface chemical state. A RTA 1 min ML deposition was analysed with XPS

technique by using a synchrotron X-Ray radiation. The collected photoelectron peaks were the Ge 3p, Sb 4p and the Ge 3d and O 1s. XPS reveals that antimony is mainly in an oxidized state, with a small metallic fraction of metallic Sb. The peak intensities trend as a function of the take-off angle indicates that an oxidized Sb layer is coating a small amount of GeO_x.
Figure 4a shows the deconvolution of the Ge 3p and Sb 4p region acquired with a photon energy of 305 eV that enhances the photoionization cross section[31].

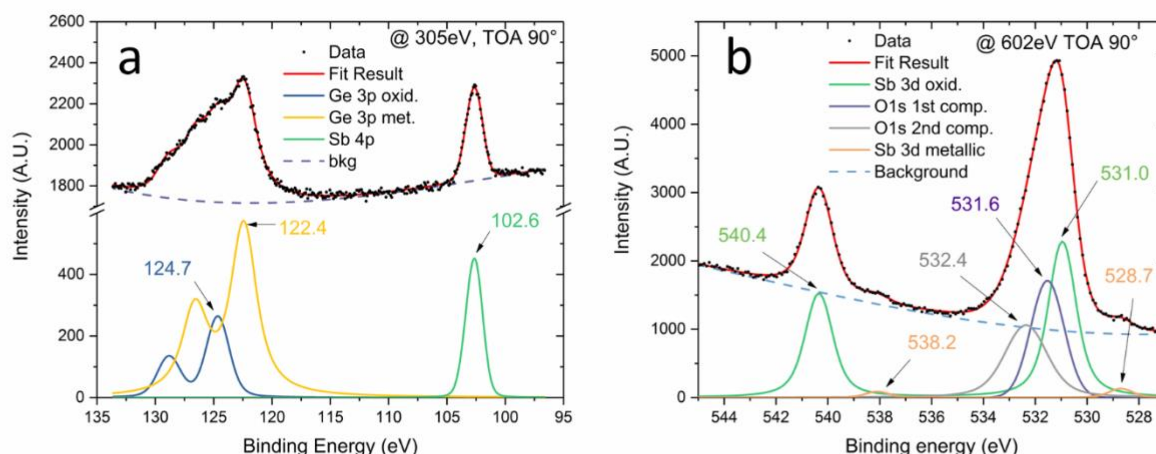

Figure 4a Ge 3p and Sb 4p signals from Sb ML on Ge (100). The spectrum was collected at normal emission conditions (90° take off angle), with a 305 eV photon energy, a pass energy of 50 eV and a 0.1 eV step.

Figure 4b O 1s Sb 3d XPS signals from Sb ML on Ge (100). The spectrum was collected at normal emission conditions (90° take off angle) with photon energy of 602 eV. For both figures, the red line is the fitted spectrum obtained by summing all the components and the background reported in the figures with different colors.

The Ge 3p region is well deconvolved by two components[32] representing metallic Ge and a Ge oxide, with the 3/2 components at 122.4 and 124.7 eV, respectively (associated peaks at lower energies are the 1/2 components). The Sb 4p 3/2 peak presents a binding energy of 102.6 eV, revealing an oxidized state of the adsorbed antimony, compatible with a +5 oxidation state[33,34]. This assignment is confirmed also by the position of the Sb 3d peak present in Figure 4b: the 3/2 component presents a binding energy of 540.4 eV, compatible with the results of Garbassi et al. [33], within the experimental error. Furthermore, the assignment of Sb(V) can be correlated with the presence of a O 1s peak at 531.6 eV. As reported in the literature[33], the oxygen bonded with Sb(V), as in the Sb_2O_5, presents a binding energy equal to 531.5 eV, compatible with our data. These data are well matched with a Sb_2O_4 assignment as well, since there is not a significant difference of chemical shift between Sb_2O_5 and Sb_2O_4 in the literature[33].
In the same binding energy region the GeO related O 1s contribution could be present, while the GeO_2 O 1s component is clearly separated and visible at 532.4 eV, in agreement with the value of 532.6 eV reported by Prabhakaran et al. [35] for the case of air oxidized Ge surface.
Thanks to the very high signal to background ratio, in this region it is even possible to notice a metallic Sb 3d component; the 3/2 and the 5/2 components are clearly present and deconvolved at 538.2 eV and 528.7 eV, respectively, and the splitting between these two peaks corresponds to the value reported in literature (9.4 eV) [33].

The Ge 3p and Sb 4p signals have been collected not only in a standard emission geometry (take off angle 90°), but also at different angles in order to study the angular dependence of the peak intensities. The intensities of Ge 3p (metallic and oxidized) and Sb 4p peaks are reported in Figure 5 as a function of the emission angle. By using the BRIXIAS code package[28], these XPS signals are analysed and their intensity variation with the angle is fitted with a multi-layer model.

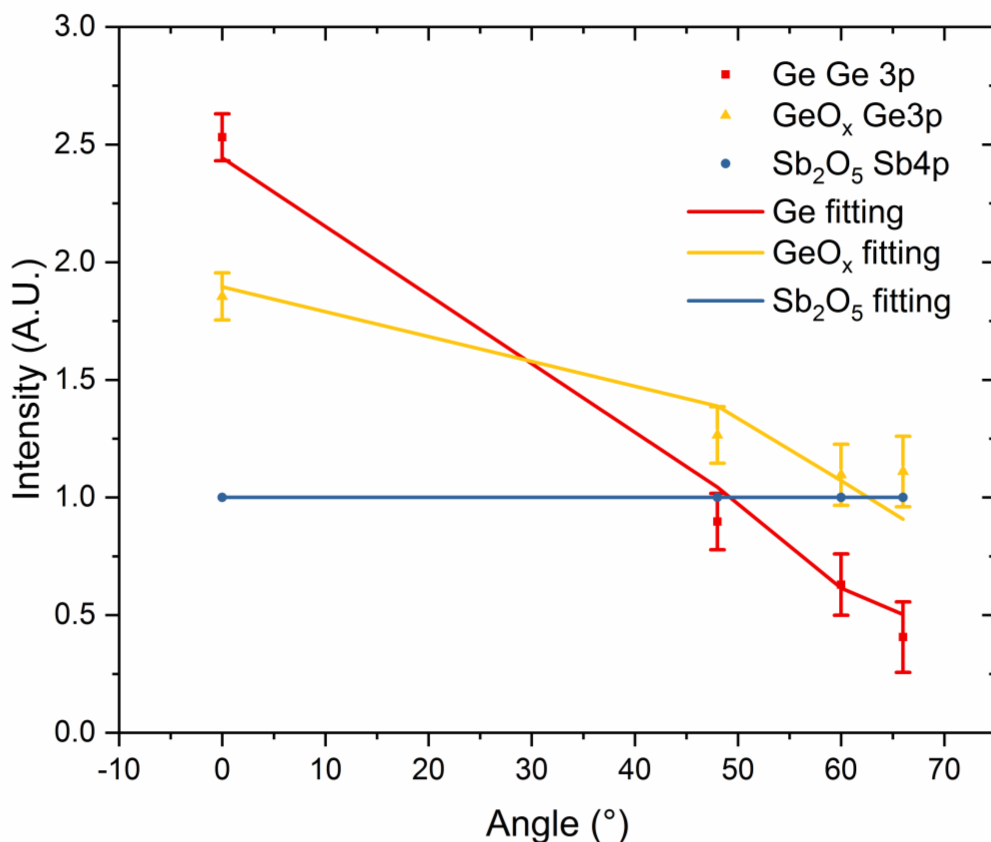

Figure 5 *Angle Resolved XPS data normalized to Sb 4p signal as a function of the emission angle, fitted by a multi-layer model with BRIXIAS code.*

The best fitting of data reported in Figure 5 is obtained by assuming the presence of 3 layers over the Ge substrate: the upper one is a carbon layer, coming from a possible contamination by atmosphere exposure. The underlying films are an antimony oxide layer and a germanium oxide layer.

The attenuation of photoelectrons (i.e. the Depth Distribution Length DDL) is calculated via Monte Carlo simulation by taking into account the multi-layer composition of the system: each layer is characterized by a specific material and thickness so that starting from an initial guess, whose parameters are adjusted during the fitting procedure, it is possible to estimate the DDL for the emitted photoelectrons and consequently the layer thickness.

A set of parameters used for the calculation is reported in *Table 1*. Even if the density of the antimony oxide and germanium oxide layers could be quite different from the bulk one, the metallic bulk germanium signals allow us to have an important reference signal to fit. Moreover, the possibility to compare the ARXPS fit results with another technique (i.e. c-RBS) can support us to validate our fitting model. The fitting result, reported in Table 1, is that the thickness of the Sb (V) layer is 2.6 Å: to compare this value with the RBS one, the thickness can be expressed in areal density

simply by transforming the layer density into an atomic density, considering the molar mass of the simulated layer. The obtained value corresponds to a surface concentration of about $4\text{x}10^{14}$ cm^{-2} Sb atoms. This value can be expressed also in terms of monolayer coverage of Ge (100) surface: taking into account that Ge (100) surface atomic density is $6.25\text{x}10^{14}$ cm^{-2} = 1ML unit, one obtains a value of 0.6 ML ($(4/6.25)\ \times 10^{14}\ cm^{-2}$ = 0.6 ML units).
This value represents the total Sb (V) amount, but not the total amount of Sb, since the Sb 3d region shows also a small Sb (0) component. By comparing the peak intensities, we obtain that the Sb (0) is about 4% of the total Sb amount.

Table 1 Properties of layers used for ARXPS analysis on Ge 3p and Sb 4p region.

E_{photon}= 305 eV	Layer composition	Tabulated layer density	Fitted thickness	Ge (100) ML units
		[g cm^{-3}]	[Å]	[ ]
	C	2.26	4.5	8.5
Sb 4p	Sb_2O_5 (V)	3.78	2.6	0.6
Ge 3p	GeO_x (II, IV)	4.70	3.8	1.7
Ge 3p	Ge (0)	5.32	bulk	bulk

The total amount of antimony estimated by ARXPS technique can be compared with c-RBS results, but remembering that the Rutherford Backscattering technique gives a dose information, while AR-XPS technique is primarily chemically sensitive and the absolute amount of Sb can be estimated only through a simulation. The c-RBS analysis gives a $5.7 \times 10^{14}\ cm^{-2}$ Sb surface areal density which corresponds to approximately 0.9 ML units ($(5.7/6.25) \times\ 10^{14}\ cm^{-2}$ = 0.9 ML units), to be compared with the 0.6 ML units obtained by AR-XPS simulation. These two values are in reasonable agreement considering that the Sb (V) layer was simulated by assuming a Sb_2O_5 density, but it could also be Sb_2O_4, as previously reported. This assumption can introduce a systematic error in the XPS dose estimation, contributing to the slight disagreement between the results of the two techniques.

Suggested monolayer adsorption mechanism

All the presented experimental evidences show a particular affinity between Sb and Ge surface during the gas phase deposition treatment. Moreover, a relatively stable oxidized Sb surface phase is present after the monolayer formation.
The synthesis process of Sb ML can be divided in two different processes that occur during the deposition: the formation of an antimony monolayer on Ge surface and the instability of Sb over-layers, both concurring to the self-limiting behavior of the whole process not to form more than one layer. These two different processes are clearly presented in the data discussed above and the instability of Sb over-layers above around 600°C is highlighted in Figure 3. Moreover, the monolayer is stable against back-decomposition toward the external environment up to the maximum Ge process temperature that is about 800°C.
In the light of all the experimental evidences, we try to infer a possible pathway for the ML formation.
It is well known in literature that antimony releases Sb_4 gas molecules as a consequence of its sublimation in an inert atmosphere not only from Sb bulk substrate[36], but also from a thin film source[37]. Moreover, the nature and the stability of the germanium surface have to be taken into

account: in fact, at the temperature at which the ML process occurs (≥ 600°C), germanium oxides start to be unstable and GeO is released[38,39].
From these information, we propose that the adsorption of Sb on the Ge surface occurs through the oxidation of Sb_4 gas by the germanium oxide according to the following reaction:

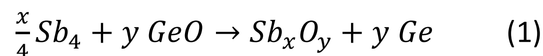

$$\frac{x}{4} Sb_4 + y\, GeO \rightarrow Sb_x O_y + y\, Ge \qquad (1)$$

The final Sb_xO_y represents the presence of Sb ML in an oxidized state, bonded with the Ge (100) surface through oxygen, as suggested by the AR-XPS analysis.
This reaction is consistent with different experimental evidences, first and foremost, the net decrease of Ge oxides after the deposition process, as clearly reported in additional info by comparing Ge 3p XPS regions of untreated and Sb ML functionalized germanium surface. By using the germanium oxide sublimation mechanism presented in literature[38], it is possible to evaluate that after 10 s at 600°C about 10^{15} cm^{-2} of GeO sublimate, and so germanium mono-oxide can act in the proposed reaction with a sufficient amount of GeO released from the surface. In particular, the GeO_2 component is eliminated from the surface owing to GeO_2 + Ge -> 2 GeO disproportionation and the subsequent sublimation of GeO [38]. Taking into account that the typical GeO_x areal density we measured by AR-XPS[5] is about 7-8 × 10^{15} cm^{-2}, it is clear that GeO is not a limiting reagent for the reaction.
The proposed adsorption reaction is also supported by thermodynamic considerations. The variation of Gibbs free energy for a given reaction ΔG_r, can be evaluated starting from the formation values ΔG_f of each reactant and product[40] at a given temperature[41]. As discussed above, GeO and Sb_4 reactants can be reasonably considered, while, as a first approximation, we can consider thermodynamic parameters for bulk Sb_2O_4 that is the stable oxide at the treatment temperature (≥ 600°C)[42] and is compatible with the previously reported XPS analysis. The resulting ΔG_r is negative and equal to -364 KJ mol^{-1} at 527°C and the values remain negative in the explored process thermal window.
A further support to the hypothesis of a GeO-induced reaction is that the Sb monolayer does not form on the Si surface as revealed by RBS analyses (see additional info Figure 2). Si native surface is characterized by a stable SiO_2 oxide. If a reaction between Sb_4 and silicon dioxide to produce Sb_2O_4 is supposed, ΔG_r turns out to be positive with a value > +1700 KJ mol^{-1} between 300-727 K, ruling out the possibility of a similar reaction on Si and explaining the peculiar behavior of Ge native surface.
The above considerations support the feasibility of a red-ox reaction between Sb_4 and GeO, although it does not take into account the surface interaction of the final product, which is expected to play a significant role. In fact, the effective structure is a self-limiting mono-layer (not a bulk) bonded to the Ge surface.
As a matter of fact, we can argument that the limiting factor for the formation of a bulk Sb_2O_4 over-layer is the finite availability of O that comes from GeO as an oxidant agent. In more detail, considering the phase diagram of Sb-O system[43], one can see that Sb_2O_4 is stable above about 600°C only if O molar fraction is above 4% (or more at higher temperature). After a first transient during GeO sublimation, GeO concentration decreases and the remaining Sb, which grows as a stable metallic layer below 600°C (Figure 2a), becomes unstable being in a liquid state[43].
We should also explain why the amount of Sb corresponds exactly to a Ge monolayer independently of the treatment conditions above 600°C. We deem that this can be explained considering that a specific interaction with the finite amount of Ge surface sites plays a role. In other words, the stable phase that really forms is a surface ternary compound with Ge-O-Sb bonds linking the Sb monolayer

with the Ge substrate. This surface phase was not previously investigated to the best of our knowledge and it could deserve further investigations by theoretical approaches to confirm its stability and structure.

Diffusion of Sb in Ge

Sb ML samples were analyzed with Secondary Ion Mass Spectrometry to evaluate the Sb in-diffusion in Ge during the deposition process and after subsequent annealing. Figure 6 shows the results of some of these analyses.

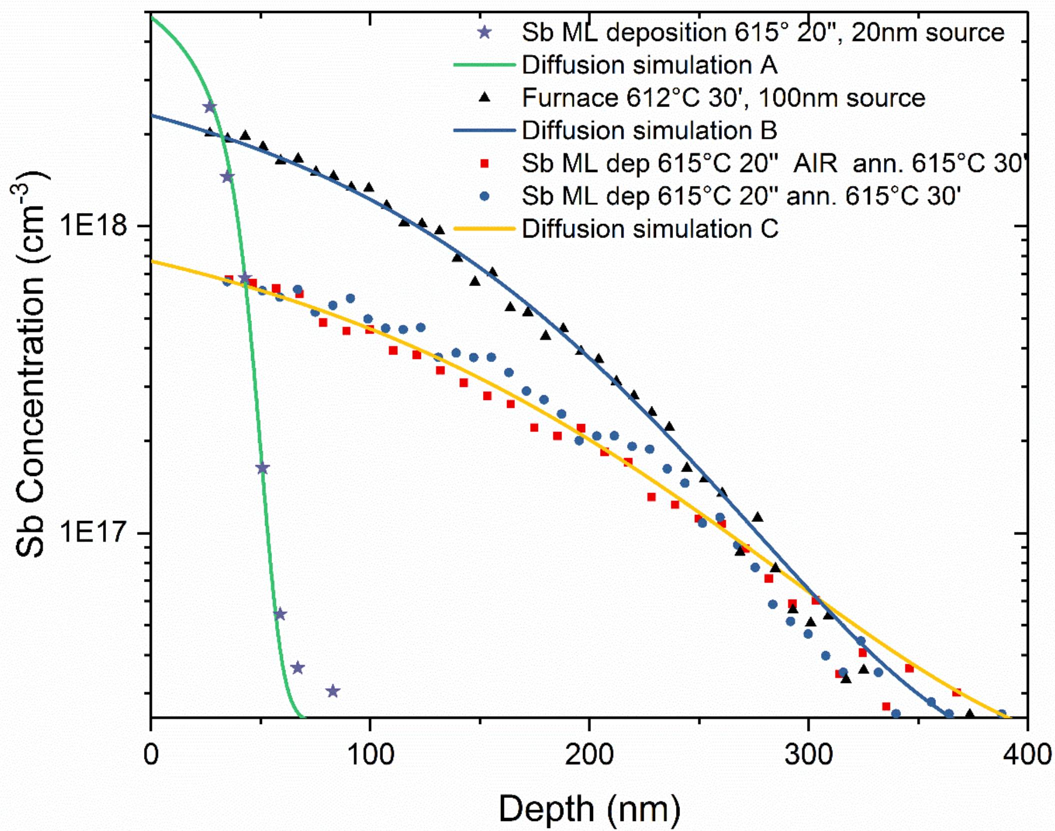

Figure 6 SIMS profile of Sb in Ge of different samples. Violet star points: 615°C 20 s Sb ML formed in RTA. Black triangles: Sb ML deposited with 612°C for 30 minutes by using a 100 nm Sb on Si source. Blue circles: Sb ML deposited via RTA 615°C 20 s and annealed at 615°C for 30 minutes without any air exposure between the two processes. Red squares: same as the previous sample but with an air exposure between the deposition and the diffusion annealing. All these data are simulated with a diffusion model as described in the text; continuous lines reported in the graph are the best simulation results.

The Sb SIMS chemical profile of a 615°C 20 s ML deposition (violet star points in Figure 6) and of a deposition at 612°C for 30 min with a standard tubular furnace (black triangles) highlight the diffusion of Sb in Ge.

In order to understand more deeply the diffusion process, all the data were simulated with a diffusion model, based on well assessed literature diffusivities data[44], using the extrinsic diffusivity model[45].
The time evolution of a Sb concentration c can be calculated by a diluted species transport equation:

$$\frac{\partial c}{\partial t} + \nabla \cdot \left(-D_{eff} \nabla \mathrm{c}\right) = 0 \qquad (2)$$

Where D_{eff} is the diffusion coefficient. According to the literature[46], the D_{eff} for n type dopants in Ge depends on carrier concentration n by means of the following equations:

$$D_{eff} = D_{Sb}^{in} \left(\frac{n(x)}{n_i}\right)^2 f \qquad (3)$$

Where D_{Sb}^{in}, determined in ref [44], is the Sb diffusivity for the case of intrinsic doping, and $(n/n_i)^2$ represents the effect of charge defect-mediated diffusion in extrinsic conditions (n(x) is the local electron concentration of determined by the doping concentration, n_i is the intrinsic carrier concentration).
f accounts for the effect of the charge species drift in the junction field, as reported in literature [23]:

$$f = \frac{2\,n(x)}{\sqrt{c^2 + 4n_i^2}} \qquad (4)$$

By numerically solving these set of equations, the Sb diffusion can be simulated both in intrinsic and extrinsic conditions. By applying this model to all the collected data reported in Figure 6, all the Sb chemical profiles are properly simulated, within a (T $\pm 10°C$) temperature and (t $\pm 2s$) time uncertainty, respectively. It is worth to note that the model closely fits the data after assuming that all the Sb is electrically active, i.e. that all the Sb in the bulk contributes to the carrier concentration n. The perfect agreement between data and simulations is a clear evidence that Sb diffuses into the bulk in a reduced state, jumping from substitutional state by interaction with vacancy present in an equilibrium concentration, as assumed in the diffusion model and previously reported in literature [47,48]. Therefore, the oxidation state of Sb inside Ge is strongly reduced with respect to the oxidized state of the Sb surface ML. This fact rules out any possible effect of O contamination on the Sb diffusion and the possibility of Sb-O co-diffusion into the bulk.

It is worth to note that only a fraction of the total Sb dose at the surface diffuses into the bulk: by integrating the SIMS chemical profiles, doses of 1.2×10^{13} cm^{-2} for the RTA 20 s 615°C sample and 1.8×10^{13} cm^{-2} for the furnace 30 minutes 612°C enter the bulk, while the surface dose is about 6.0×10^{14} cm^{-2} for both samples according to c-RBS measurements reported in Figures 2 and 3.
In order to understand the role played by the oxidized Sb surface ML in the bulk Sb injection, we tried to further anneal the RTA 20 s 615°C sample with a second process for 30 minutes at 615°C. The resulting chemical profile is also reported in Figure 6 (red squares).
The diffusion profile can be perfectly simulated by assuming that the Sb diffused after 20 s (violet star points in Figure 6) further diffuse for 30 minutes at equilibrium without any Sb loss or injection through the surface. As a matter of fact, the Sb dose in this sample is 1.2×10^{13} cm^{-2} just like after the first step, thus demonstrating that no contribution comes from the oxidized Sb surface monolayer, which appears to be rather a barrier to Sb out diffusion.

We can argue that the diffusing Sb under standard annealing procedures is a reduced Sb that appears below the surface during the formation of the monolayer and is revealed by XPS as the small metallic Sb peak shown in Figure 4b.
In Figure 6 we can notice that the single step 30 minutes annealed sample (black points) has a higher Sb concentration with respect to the two steps sample (red points). The differences between the two samples are the air exposure between the two annealing treatments for the two-step sample and the longer Sb exposure during the annealing for the single step sample (the latter was produced with a 100 nm source instead of a 20 nm used for the two steps). In order to understand what the dominating factor is, we repeated the two steps annealing by doing the second annealing without air exposure and after cleaning the RTA oven by N_2 flux and vacuum cycles. Taking into account that after the first step the 20 nm source is completely exhausted (see previous RBS results), the presence of Sb gas in the chamber during the second annealing is absolutely ruled out.
The result is represented by blue circles in Figure 6 and is identical to the two steps annealing with air exposure (red data). This demonstrates that air exposure does not influence the process and this is compatible with the idea that the diffusing Sb is already embedded into Ge after 20 s. We can therefore conclude that the longer Sb gas exposure stimulates the Sb injection into the bulk at a higher concentration.

In summary standard diffusion annealing demonstrates that only a fraction of the deposited Sb is able to diffuse into Ge and that this diffusion still occurs during short ML formation processes. The data are well reproduced by equilibrium concentration diffusion of fully active Sb and the fast diffusion in a first short period can be explained by the non-linear term in diffusivity that results to be higher at the higher concentration at the beginning of the process. The diffusing component appears to be a direct transfer of reduced Sb from gas to the bulk and no evidence of Sb release from the oxidized monolayer was found under the investigated equilibrium thermal processes.
It could be interesting to further investigate very short time and higher temperature gas exposure by close source, developing special experimental set-up for this aim. This could lead to the formation of shallow junctions at higher concentration and with shorter length, but it does not seem to take advantage from the deposited ML as a local dopant source.
In the following we demonstrate as the whole ML can act as a source by exploiting PLM treatments.

Non-equilibrium Sb diffusion in Ge

Here we report a doping process performed starting from the Sb ML source under a highly non-equilibrium condition. A Sb ML, formed with RTA 20 s 600°C, is treated with Pulsed Laser Melting technique [49]. As described in the experimental section, one high energy density laser pulse melts the Ge surface (about 150 nm thick) and consequently Sb can diffuse in liquid Ge[50]. After a certain delay, Ge recrystallizes epitaxially from the liquid/solid interface and Sb is then englobed in Ge [51]. In Figure 7, a SIMS profile of Sb diffused in Ge after a PLM 1 pulse treatment is reported.

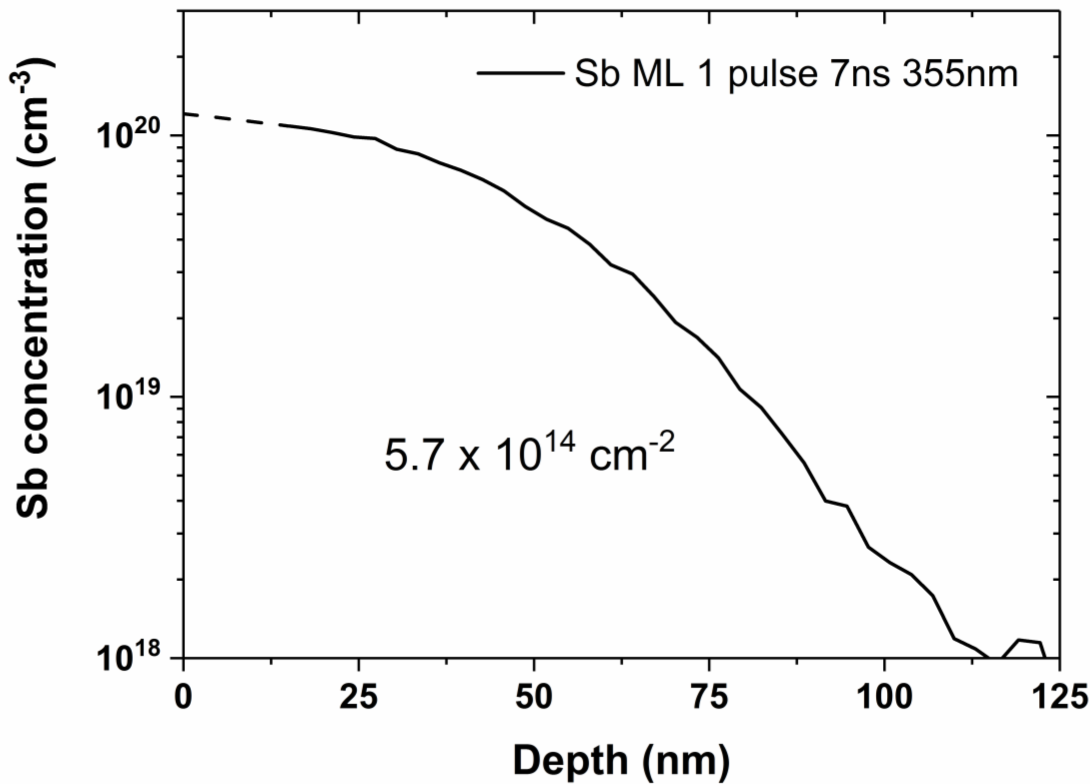

Figure 7 *SIMS chemical profile of Sb ML diffused with PLM technique: 1 pulse of 7 ns at 355 nm photon wavelength. The line is truncated near the surface since in this region the SIMS signal can be affected by surface effect. The total dose, obtained by integrating the SIMS profile, is reported in the figure.*

As shown in Figure 7, the antimony diffuses in germanium generating a typical diffusion profile of PLM treated sample [18]. It is clearly evident that a high concentration of Sb in Ge is reached, with a surface concentration of 1.2×10^{20} cm^{-3}, well above the maximum equilibrium solid solubility ($1.3\text{x}10^{19}$ cm^{-3}) of Sb in Ge [52] and previous results presented in this work (Figure 6). As evaluated by laser induced melting calculations (LIMP - the Harvard simulation software package[53] based on heat flow calculation calibrated on Ge physical and optical literature data) the PLM process at the used energy density is expected to melt for about 30 ns and up to a depth around 150 nm. This is fully compatible with our result, since the diffused Sb profile is shallower than 150 nm and does not show any shoulder typical of diffusion limited by the maximum melt-depth. Such shoulder would have been originated indeed by the diffusion coefficient in solid, whose value is orders of magnitude lower than in liquid. Thus, the Sb diffusion behavior revealed by the data of this paper points to a limitation induced by the Ge liquid diffusivity rather than the maximum melt-depth. Furthermore, an estimation of the Sb diffusivity considering the calculated melt time of 30 ns and the observed profile depth at half maximum gives an order of magnitude of 10^{-4} cm^2/s, which is in agreement with the values reported in literature for the diffusivity of dopants in liquid Ge [26].
By integrating the SIMS profile, one obtains that the areal density of Sb diffused in Ge is 5.7×10^{14} cm^{-2}, that is the same value of the surface Sb ML, thus demonstrating that all the available Sb diffused under PLM.
In order to verify the electrical properties of the doped layer, van der Pauw-Hall measurement allows to determine the Hall Coefficient that depends on the carriers sign and areal density [54]. The Hall Coefficient measured for this sample is -1.45×10^4 cm^2/C. Considering a full electrical activation

of the diffused Sb (i.e. each Sb atom produces one electron carrier), Hall coefficient can be also calculated by exploiting the procedure reported in Ref. [55,56] and results to be -1.53×10^{4} cm^2/C. On the basis of the very good agreement between measured and calculated values, we can conclude that all the Sb is fully electrically active within the experimental errors.

Furthermore, the same set-up allows to measure the sheet resistance that depends on both the carrier concentration profile and the mobility. Having demonstrated that the carrier concentration profile is overlapped to the Sb profile, the mobility can be deduced with a similar procedure [55,56] obtaining a value of 208 $cm^2V^{-1}s^{-1}$ at the maximum concentration of 1.2×10^{20} cm^{-3} , in very good agreement with literature data for Ge doped with the same Sb concentration (218 $cm^2V^{-1}s^{-1}$) [57].

These interesting results show that the PLM technique is able to promote the diffusion of the whole Sb ML, by reducing the oxidized Sb ML fraction without any Sb loss during the process. The full electrical activation of the layer demonstrates that no detrimental effect of O present in the ML structure occurs in the junction. This could be indeed expected taking into account the small O amount in the ML structure (only 3 Å thick) as compared to that in the native GeO_x (in the order of 20 Å).

This experiment shows that Sb ML acts as a dopant source also for PLM technique and one can foresee that a further laser parameter optimization, such as the use of a different laser energy, should reduce the junction thickness and consequently raise the Sb concentration in Ge. The creation of shallow junctions in germanium using PLM method was already proved in literature [58], thanks to the fact that by tuning the energy density of laser, the maximum melt depth can be finely modified [50,51,59]. Therefore, the preliminary result shown in Figure 7 can be improved, reducing the junction thickness (down to the as deposited one) and consequently increasing the Sb concentration.

Conclusions

In this paper, a self-limited formation of an antimony monolayer on Ge (100) surface has been demonstrated and analyzed with different techniques. A wide range of formation parameters has been examined such as time, temperature and deposition atmosphere. They reveal a self-limiting formation with wide thermal windows, a very good areal uniformity and an extremely fast ML formation.

XPS chemical characterization discloses that antimony is mainly in an oxidized layer, bonded with Ge bulk through a very thin Ge oxide layer. Moreover, a small but significant fingerprint of the presence of reduced Sb on top of bulk Ge is clearly revealed and quantified.

On these bases, we proposed a red-ox mechanism between Sb and Ge oxide for the formation of antimony monolayer and we supported this hypothesis also with thermodynamic considerations.

The self-limiting behavior of the entire process is explained by considering the stability of Sb-O system under variable oxidizing agent concentrations and suggesting a specific role of the surface in the formation of a Ge-O-Sb surface phase.

SIMS characterization on functionalized Ge detects the presence of an antimony fraction able to diffuse and dope Ge under equilibrium thermal conditions. The diffusion of Sb can be modeled with the well assessed equilibrium diffusion of Sb, unveiling a Sb diffusing in a reduced state in the Ge matrix. Finally, an out-equilibrium process exploiting the innovative Sb source is demonstrated reaching a Sb n-doping of Ge with a 100% electrical activation and a very high concentration by using all the oxidized Sb ML as a dopant source.

As compared to classical ML doping techniques, this new promising deposition approach features several remarkable strengths, such as: i) complex chemical reactions, eventually needed for the

synthesis of the Sb molecular precursor and its functionalization with a proper functional group are completely avoided; ii) the incorporation of any residual molecular fragments that can act as contaminants in germanium is also averted; iii) one-step process by deposition and diffusion of Sb at the same time is possible; iv) seconds-time scale Sb ML formation; v) thermal removal of the native germanium oxide by sublimation (avoiding a strong acid dissolution process) and a following stabilization of the surface by Sb itself.

Acknowledgements

The authors are thankful to Luca Bacci (University of Padova) for technical assistance during RBS measurements and Nicola Argiolas (University of Padova) for AFM measurements. Daniele Scarpa and Alberto Andrighetto (INFN Laboratori Nazionali di Legnaro) are acknowledged for support during the laser annealing processes.
We thank the Elettra synchrotron S.c.P.A. for the user support received for the proposal n.20175477.
This project has received funding from the European Union Horizon 2020 research and innovation program under the grant agreement n. 654002.

Bibliography

1. Various_Authors. *ITRS for Semiconductor 2015*.; 2015. https://www.semiconductors.org/wp-content/uploads/2018/06/0_2015-ITRS-2.0-Executive-Report-1.pdf.
2. Cho K, Ruebusch DJ, Lee MH, et al. Molecular monolayers for conformal, nanoscale doping of InP nanopillar photovoltaics. *Appl Phys Lett*. 2011;98(20):1-4. doi:10.1063/1.3585138
3. Simoen E, Satta A, D'Amore A, et al. Ion-implantation issues in the formation of shallow junctions in germanium. *Mater Sci Semicond Process*. 2006;9(4-5 SPEC. ISS.):634-639. doi:10.1016/j.mssp.2006.08.067
4. Connell JO, Biswas S, Duffy R. Chemical approaches for doping nanodevice architectures. *Nanotechnology*. 2016;27(342002). doi:10.1088/0957-4484/27/34/342002
5. Sgarbossa F, Carturan SM, De Salvador D, et al. Monolayer doping of germanium by phosphorus containing molecules. *Nanotechnology*. 2018;29(465702). doi:10.1088/1361-6528/aade30
6. Ho JC, Yerushalmi R, Smith G, et al. Wafer-Scale , Sub-5 nm Junction Formation by Monolayer Doping and Conventional Spike Annealing. *Nano Lett*. 2009;9(2):5-10. doi:10.1021/n18032526
7. Ang KW, Barnett J, Loh WY, et al. 300mm FinFET results utilizing conformal, damage free, ultra shallow junctions (X j~5nm) formed with molecular monolayer doping technique. *Tech Dig - Int Electron Devices Meet IEDM*. 2011:837-840. doi:10.1109/IEDM.2011.6131679
8. Ye L, González-Campo A, Kudernac T, et al. Monolayer Contact Doping from a Silicon Oxide Source Substrate. *Langmuir*. 2017;33(15):3635-3638. doi:10.1021/acs.langmuir.7b00157

9. Hazut O, Agarwala A, Amit I, et al. Contact doping of silicon wafers and nanostructures with phosphine oxide monolayers. *ACS Nano*. 2012;6(11):10311-10318. doi:10.1021/nn304199w
10. Hazut O, Yerushalmi R. Direct Dopant Patterning by a Remote Monolayer Doping Enabled by a Monolayer Fragmentation Study. *Langmuir*. 2017;33(22):5371-5377. doi:10.1021/acs.langmuir.7b01085
11. Alphazan T, Diaz Alvarez A, Martin F, et al. Shallow heavily-doped n++ germanium by organo-antimony monolayer doping. *ACS Appl Mater Interfaces*. 2017;9:20179-20187. doi:10.1021/acsami.7b02645
12. Long B, Alessio Verni G, O'Connell J, et al. Molecular Layer Doping : Non-destructive Doping of Silicon and Germanium. In: *Ion Implantation Technology (IIT), 2014 20th International Conference On*. Cork, Ireland: IEEE; 2014. doi:10.1109/IIT.2014.6939995
13. Kim Y, Lam ND, Kim K, Park W-K, Lee J. Ge nanopillar solar cells epitaxially grown by metalorganic chemical vapor deposition. *Sci Rep*. 2017;7:42693. doi:10.1038/srep42693
14. Wang D, Chang YL, Wang Q, et al. Surface chemistry and electrical properties of germanium nanowires. *J Am Chem Soc*. 2004;126(37):11602-11611. doi:10.1021/ja047435x
15. Pillarisetty R. Academic and industry research progress in germanium nanodevices. *Nature*. 2011;479(7373):324-328. doi:10.1038/nature10678
16. Süess MJ, Geiger R, Minamisawa RA, et al. Analysis of enhanced light emission from highly strained germanium microbridges. *Nat Photonics*. 2013;7(6):466-472. doi:10.1038/nphoton.2013.67
17. Carroll L, Friedli P, Neuenschwander S, et al. Direct-gap gain and optical absorption in germanium correlated to the density of photoexcited carriers, doping, and strain. *Phys Rev Lett*. 2012;109(5):1-5. doi:10.1103/PhysRevLett.109.057402
18. Maggioni G, Carturan S, Raniero W, et al. Pulsed laser di ff usion of thin hole-barrier contacts in high purity germanium for gamma radiation detectors. *Eur Phys J A*. 2018;54(34). doi:10.1140/epja/i2018-12471-0
19. Frigerio J, Ballabio A, Isella G, et al. Tunability of the dielectric function of heavily doped germanium thin films for mid-infrared plasmonics. *Phys Rev B - Condens Matter Mater Phys*. 2016;94(8):1-18. doi:10.1103/PhysRevB.94.085202
20. Petykiewicz J, Nam D, Sukhdeo DS, et al. Direct Bandgap Light Emission from Strained Germanium Nanowires Coupled with High-Q Nanophotonic Cavities. *Nano Lett*. 2016;16(4):2168-2173. doi:10.1021/acs.nanolett.5b03976
21. Wan KJ, Ford WK, Hermanson JC. Observation and LEED I-V analysis of the Ge(111)-1×1-Sb system. *Surf Sci*. 1992;268(1-3). doi:10.1016/0039-6028(92)90930-5
22. Kendelewicz T, Woicik JC, Miyano KE, et al. Structure of Sb monolayers on Ge(111)2×1: A combined study using core-level photoemission, x-ray standing waves, and surface extended x-ray absorption fine structure. *J Vac Sci Technol B Microelectron Nanom Struct*. 1993;11(4):1449. doi:10.1116/1.586958
23. Maggioni G, Sgarbossa F, Napolitani E, et al. Diffusion doping of germanium by sputtered antimony sources. *Mater Sci Semicond Process*. 2018;75(November 2017):118-123. doi:10.1016/j.mssp.2017.11.026
24. Boldrini V, Carturan SM, Maggioni G, et al. Optimal process parameters for phosphorus spin-on-doping of germanium. *Appl Surf Sci*. 2016;392:1173-1180. doi:10.1016/j.apsusc.2016.09.134
25. Impellizzeri G, Napolitani E, Boninelli S, et al. B-doping in Ge by excimer laser annealing. *J Appl Phys*. 2013;113(11). doi:10.1063/1.4795268
26. Milazzo R, Napolitani E, Impellizzeri G, et al. N-type doping of Ge by As implantation and excimer laser annealing. *J Appl Phys*. 2014. doi:10.1063/1.4863779

27. Frigerio J, Ballabio A, Gallacher K, et al. Optical properties of highly n-doped germanium obtained by in situ doping and laser annealing. *J Phys D Appl Phys*. 2017;50(46). doi:10.1088/1361-6463/aa8eca
28. Drera G, Salvinelli G, Åhlund J, et al. Transmission function calibration of an angular resolved analyzer for X-ray photoemission spectroscopy: Theory vs experiment. *J Electron Spectros Relat Phenomena*. 2014;195:109-116. doi:10.1016/j.elspec.2014.06.010
29. Salvinelli G, Drera G, Baratto C, Braga A, Sangaletti L. Stoichiometry gradient, cation interdiffusion, and band alignment between a nanosized TiO2 blocking layer and a transparent conductive oxide in dye-sensitized solar cell front contacts. *ACS Appl Mater Interfaces*. 2015;7(1):765-773. doi:10.1021/am5072018
30. Boldrini V, Maggioni G, Carturan S, et al. Characterization and modeling of thermally-induced doping contaminants in high-purity Germanium. *J Phys D Appl Phys*. 2019;52(035104):11. doi:10.1088/1361-6463/aae9c0
31. Yeh JJ, Lindau I. Atomic Subshell Photoionization Cross Sections and Asymmetry Parameters. *At Data Nucl Data Tables*. 1985;32(l):1-155. doi:10.1016/0092-640X(85)90016-6
32. Xie Q, Deng S, Schaekers M, et al. Germanium surface passivation and atomic layer deposition of high-k dielectrics - A tutorial review on Ge-based MOS capacitors. *Semicond Sci Technol*. 2012;27(7). doi:10.1088/0268-1242/27/7/074012
33. Garbassi F. XPS and AES study of antimony oxides. *Surf Interface Anal*. 1980;2(5):165-169. doi:10.1002/sia.740020502
34. Izquierdo R, Sacher E, Yelon A. X-ray photoelectron spectra of antimony oxides. *Appl Surf Sci*. 1989;40(1-2):175-177. doi:10.1016/0169-4332(89)90173-6
35. Prabhakaran K, Ogino T. Oxidation of Ge(100) and Ge(111) surfaces: an UPS and XPS study. *Surf Sci*. 1995;325(3):263-271. doi:10.1016/0039-6028(94)00746-2
36. Rosenblatt GM, Lee P-K. Vaporization Kinetics and Thermodynamics of Antimony and the Vaporization Coefficient of Antimony Single Crystals. *J Chem Phys*. 1970;52(1454):1454-1464. doi:10.1063/1.1673150
37. Sommer AH. Characteristics of evaporated antimony films as a function of the antimony source. *J Appl Phys*. 1966;37(7):2789-2791. doi:10.1063/1.1782124
38. Pauleau Y, Remy JC. Kinetics of the formation and sublimation of germanium monoxide. *J Less-Common Met*. 1975;42(2):199-208. doi:10.1016/0022-5088(75)90005-3
39. William B, Jolly L, Latimer WM. The Equilibrium Ge + GeO2 = 2 GeO. The Heat of Formation of Germanic. *J Am Chem Soc*. 1952;74(22):5757-5758. doi:10.1021/ja01142a056
40. Barin I. *Thermochemical Data of Pure Substances*.
41. Atkins P, De Paula J. *Physical Chemistry*. eight edit. W.H. Freeman and Company, New York; 2006.
42. Cody CA, Dlcarlo L, Darlington RK. Vibrational and Thermal Study of Antimony Oxides. *Inorg Chem*. 1979;18(6):1572-1576. doi:10.1021/ic50196a036
43. Asryan NA, Alikhanyan AS, Nipan GD. P-T-x phase diagram of the Sb-O system. *Inorg Mater*. 2004;40(6):626-631. doi:10.1023/B:INMA.0000031997.59271.0f
44. Brotzmann S, Bracht H. Intrinsic and extrinsic diffusion of phosphorus, arsenic, and antimony in germanium. *J Appl Phys*. 2008;103:033508. doi:10.1063/1.2837103
45. Chroneos A, Bracht H. Diffusion of n -type dopants in germanium. *Appl Phys Rev*. 2014;1(1). doi:10.1063/1.4838215
46. Pichler P. *Intrinsic Point Defects, Impurities, and Their Diffusion in Silicon*.; 2004. doi:10.1007/978-3-7091-0597-9
47. Chroneos A, Bracht H, Grimes RW, Uberuaga BP. Vacancy-mediated dopant diffusion

activation enthalpies for germanium. *Appl Phys Lett*. 2008;92(17):1-4. doi:10.1063/1.2918842

48. Brotzmann S, Bracht H, Hansen JL, et al. Diffusion and defect reactions between donors, C, and vacancies in Ge. I. Experimental results. *Phys Rev B - Condens Matter Mater Phys*. 2008;77(23):1-13. doi:10.1103/PhysRevB.77.235207
49. Poate J, Mayer JW. *Laser Annealing of Semiconductors*. Elsevier; 1982.
50. Wood RF, Giles GE. Macroscopic theory of pulsed-laser annealing. I. Thermal transport and melting. *Phys Rev B*. 1981;23(6):2923-2942.
51. Wood RF, Kirkpatrick JR, Giles GE. Macroscopic theory of pulsed-laser annealing. II. Dopant diffusion and segregation. *Phys Rev B*. 1981;23(10):5555-5569. doi:10.1103/PhysRevB.23.5555
52. Trumbore FA. Solid Solubilities of Impurity Elements in Germanium and Silicon. *Bell Syst Tech J*. 1960;39(1):205-233. doi:10.1002/j.1538-7305.1960.tb03928.x
53. Hoglund DE, Thompson MO, Aziz MJ. Experimental test of morphological stability theory for a planar interface during rapid solidification. *Phys Rev B - Condens Matter Mater Phys*. 1998;58(1):189-199. doi:10.1103/PhysRevB.58.189
54. van der Pauw LJ. A method of measuring the resistivity and Hall coefficient on lamellae of arbitrary shape. *Philips Tech Rev*. 1958;20:220-224.
55. Petritz RL. Theory of an experiment for measuring the mobility and density of carriers in the space-charge region of a semiconductor surface. *Phys Rev*. 1958;110(6):1254-1262. doi:10.1103/PhysRev.110.1254
56. Baron R, Shifrin GA, Marsh OJ, Mayer JW. Electrical behavior of group III and V implanted dopants in silicon. *J Appl Phys*. 1969;40(9):3702-3719. doi:10.1063/1.1658260
57. Xu C, Senaratne CL, Sims P, Kouvetakis J, Menéndez J. Ultralow Resistivity Ge:Sb heterostructures on Si Using Hydride Epitaxy of Deuterated Stibine and Trigermane. *ACS Appl Mater Interfaces*. 2016;8(36):23810-23819. doi:10.1021/acsami.6b06161
58. Heo S, Baek S, Lee D, et al. Sub-15 nm n[sup +]⁄p-Germanium Shallow Junction Formed by PH[sub 3] Plasma Doping and Excimer Laser Annealing. *Electrochem Solid-State Lett*. 2007;9(4):G136. doi:10.1149/1.2172470
59. Surko CM, Simons L, Auston DH, Golovchenko JA, Slusher RE. Calculation of the dynamics of surface melting during laser annealing. *Appl Phys Lett*. 1979;34(10):635-637. doi:10.1063/1.90619

1
2
3
4
5
6
7
8
9
10
11
12
13
14
15
16
17
18
19
20
21
22
23
24
25
26
27
28
29
30
31
32
33
34
35
36
37
38
39
40
41
42
43
44
45
46
47
48
49
50
51
52
53
54
55
56
57
58
59
60
61
62
63
64
65

Supplementary Information
Self-limiting Sb monolayer as a diffusion source for Ge doping.

Francesco Sgarbossa; Gianluigi Maggioni; Gian Andrea Rizzi;
Sara Maria Carturan; Enrico Napolitani; Walter Raniero;
Chiara Carraro; Federica Bondino; Igor Pis; Davide De Salvador

1
2
3
4
5
6
7
8
9
10
11
12
13
14
15
16
17
18
19
20
21
22
23
24
25
26
27
28
29
30
31
32
33
34
35
36
37
38
39
40
41
42
43
44
45
46
47
48
49
50
51
52
53
54
55
56
57
58
59
60
61
62
63
64
65

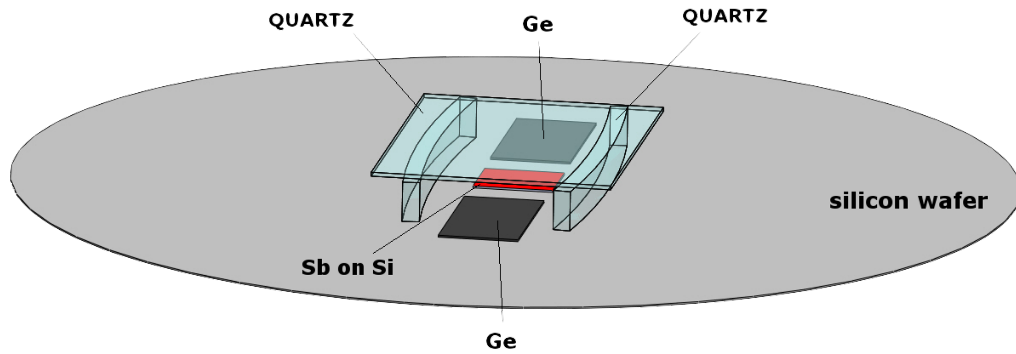

Figure 1: Sample scheme in the Rapid Thermal Process furnace process (RTA). The metallic Sb deposited via sputtering on Si support, called source sample, is drawn in red and the Sb deposited faced up. The Ge target samples are drawn in black and placed near the source sample; the quartz spacer and the upper quartz windows are placed on the sides and above the source sample to prevent the Sb direct flooding on the RTA cold wall. Quartz is almost perfectly transparent to the lamp radiation allowing the heating of the sample as confirmed by thermal simulation of the system. A very good thermal contact is ensuring between the source, Ge samples and the supporting Si wafer by the perfect contact between their double polish cutting quality faces.

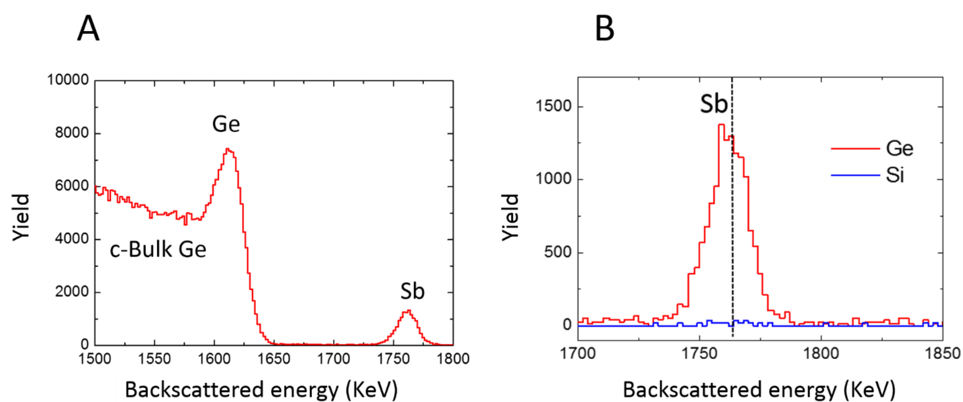

Figure 2:
Figure 2 A: c-RBS signals coming from a channeled Ge (100) substrate after a Sb deposition.
Figure 2 B: The comparison between a Sb ML signal and a Sb exhausted source on Si substrate in a 560°C for 30 min treatment in the tubolar furnace. The vertical dotted line rappresents the Sb kE_0 i.e. the teoretical position in energy of backscattered particles coming from Sb positioned on the surface of the sample.

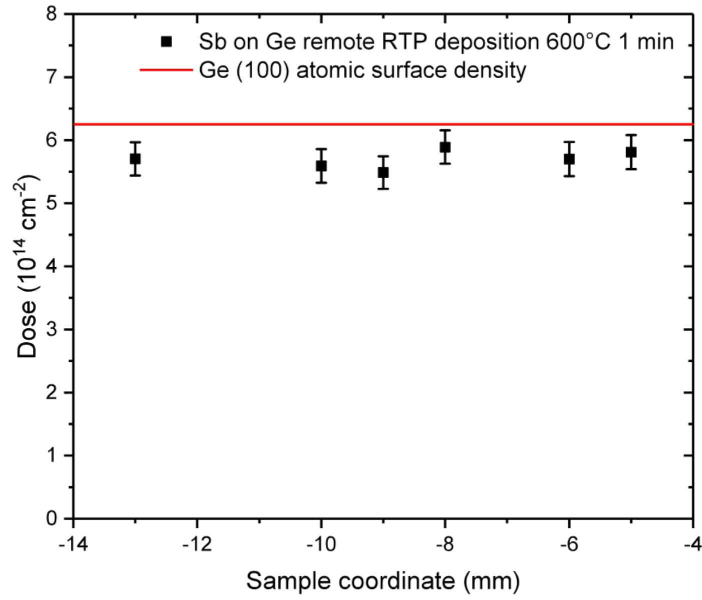

Figure 3: RBS doses of antimony deposition via RTA (600°C for 1 minute deposition); homogeneity of Sb ML along Ge (100) surface.

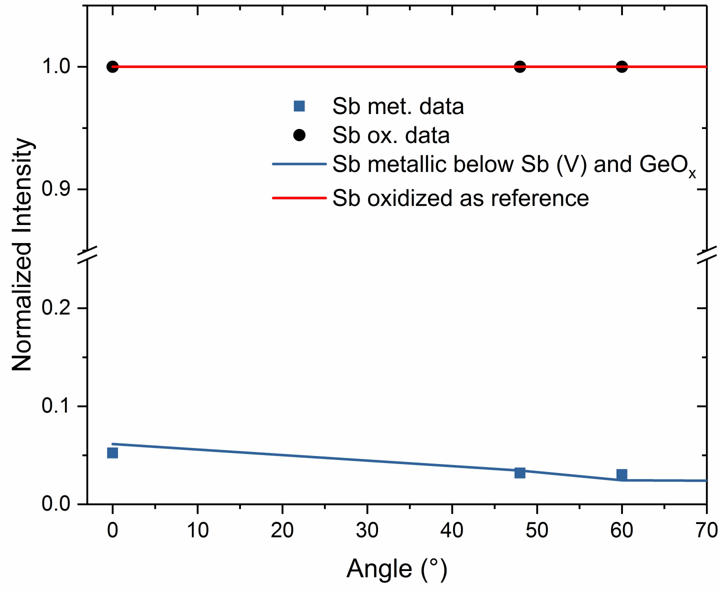

Figure 4: Metallic Sb peak intensity trend with take-off angle.

1
2
3
4
5
6
7
8
9
10
11
12
13
14
15
16
17
18
19
20
21
22
23
24
25
26
27
28
29
30
31
32
33
34

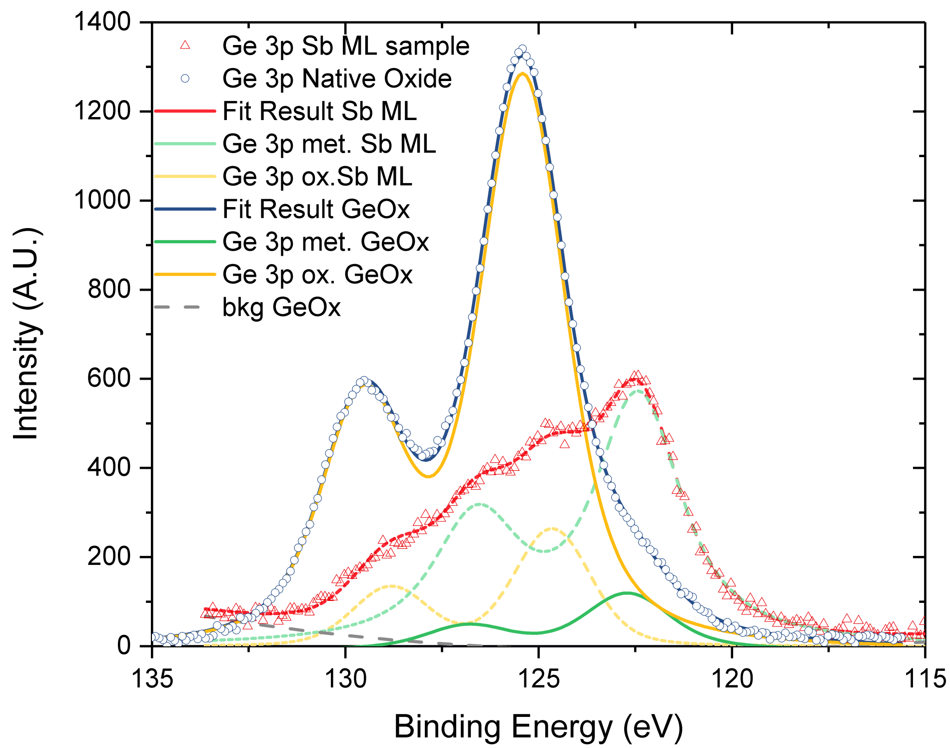

35
36
37
38
39
40
41

Figure 5: XPS Ge 3p regions of: Sb ML deposited at 600°C for 1 min via RTA in red triangles and a germanium sample before any treatments (presenting a native oxide layer, as before the ML deposition treatment) in blue circles. The two spectra were deconvolved with a metallic and an oxide component, green and yellow line respectively, as reported in the article.

42
43
44
45
46
47
48
49
50
51
52
53
54
55
56
57
58

59
60
61
62
63
64
65

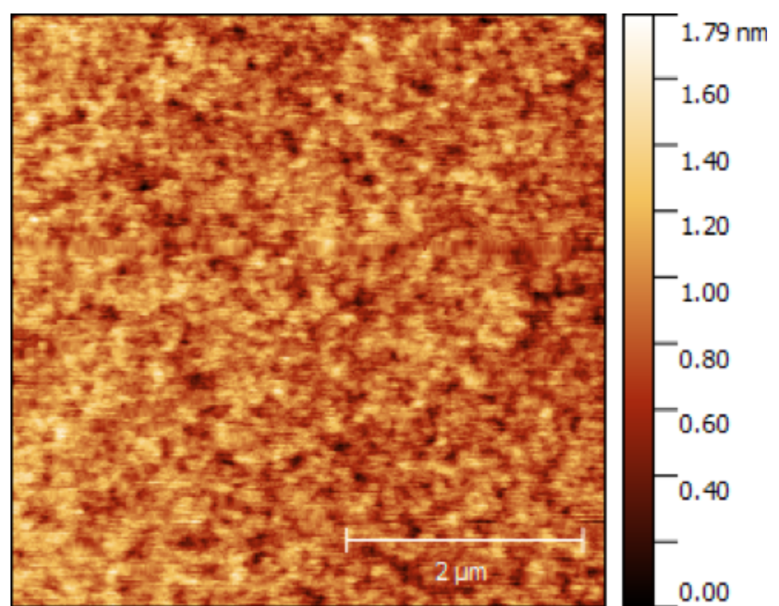

Figure 6: 5x5 μm AFM image of antimony monolayer deposited via RTA for 1 minute at 600 Celsius. Calculated roughness 1.8 Angstrom. The image was acquired with DI Cp-II AFM instrument using a commercial silicon nitride cantilever.

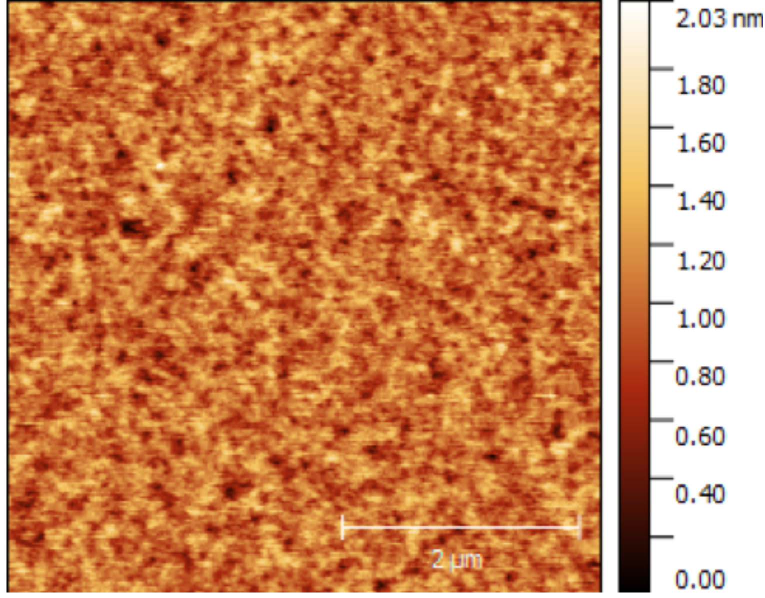

Figure 7: 5x5 μm AFM image of an untreated Ge (100) surface, the starting material for Sb ML deposition. Calculated roughness 1.9 Angstrom. The image was acquired with DI Cp-II AFM instrument using a commercial silicon nitride cantilever.

Calculation of $\Delta_r G$ for the proposed injection mechanism

The $\Delta_r G^{\ominus}$ is calculated from the following equation:

$$\Delta_r G^{\ominus} = \sum_{Products} \nu \Delta_f G^{\ominus} - \sum_{Reactants} \nu \Delta_f G^{\ominus} \tag{1}$$

or more formally:

$$\Delta_r G^{\ominus} = \sum_j \nu_j \Delta_f G_j^{\ominus} \tag{2}$$

Since the reaction occurs not in standard conditions, the $\Delta_r G$ must be evaluated at a certain T. For this reason, equation 2 can be expressed also at different temperature:

$$\Delta_r G(T) = \sum_j \nu_j \Delta_f G_j(T) \tag{3}$$

The supposed adsorption chemical reaction is balanced as follow:

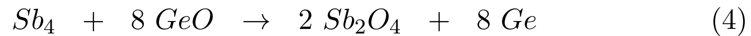

$$Sb_4 \quad + \quad 8\ GeO \quad \rightarrow \quad 2\ Sb_2O_4 \quad + \quad 8\ Ge \tag{4}$$

The $\Delta_r G$ for the given reaction is calculated starting from tabulated values present in *Thermochemical Data of Pure Substances* by Ihsan Barin for Sb_4, Sb_2O_4 and GeO. The Ge is considered in its standard element state and for this reason the $\Delta_f G(Ge) = 0$ at different temperatures. The $\Delta_r G(T)$ for the given reaction gives $-677\ KJ\ mol^{-1}$ at $600K$, and $-210\ KJ\ mol^{-1}$ at $900K$.

The evaluation $\Delta_r G(T)$ for the red-ox reaction between Sb_4 and SiO_2 is evaluated considering the following reaction:

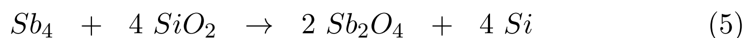

$$Sb_4 \ + \ 4\ SiO_2 \ \rightarrow \ 2\ Sb_2O_4 \ + \ 4\ Si \tag{5}$$

The $\Delta_r G(T)$ for the given reaction gives $+1720\ KJ\ mol^{-1}$ at $600K$, and $+1793\ KJ\ mol^{-1}$ at $1000K$.

Supplementary Material for on-line publication only
Click here to download Supplementary Material for on-line publication only: add_info.pdf